CrossMark

TMS2017 HIGHLIGHTS

Deformation of Heterogeneous Nanocrystalline Lamella with a Preexisting Crack

SIXIE HUANG, 1 JIAN WANG, 2 and CAIZHI ZHOU 1,3,4

1.—Department of Materials Science and Engineering, Missouri University of Science and Technology, Rolla, MO 65409, USA. 2.—School of Civil Engineering, Southwest Jiaotong University, Chengdu 610031, People's Republic of China. 3.—Department of Mechanical and Aerospace Engineering, Missouri University of Science and Technology, Rolla, MO 65409, USA. 4.—e-mail: zhouc@mst.edu

Molecular dynamics simulations were performed on heterogeneous nanocrystalline Al lamellae composed of nanocrystalline (NC) and single-crystalline (SC) layers to study the effect of the heterogeneous microstructures on the propagation of preexisting cracks. Under tensile loading, the heterogeneous NC Al lamella exhibited higher crack growth resistance than the pure NC Al. In addition, a lower volume fraction of the NC layer provided better crack growth resistance in heterogeneous lamellae (HL) samples, which agrees well with previous experiment results. After analyzing the distribution of the atom-level virial stress and microstructure evolution during the deformation, we found that the average stress on grain boundary atoms was much lower in HL samples than that in pure NC sample. When the crack approaches the interface, the heterogeneous microstructure can reduce the stress concentration by emitting dislocations from the interface into the SC layer.

INTRODUCTION

Extensive investigations have been carried out on nanocrystalline (NC) materials over the past decades as a result of their ultra-high-strength and wear resistance.^{1,2} Nevertheless, the uniform elongation of NC materials is limited to a few percent and usually decreases with the grain size. Recently, heterogeneous lamella (HL) structures characterized with alternating lamellae of soft micro grains and hard ultrafine/nano grains attract growing attention in the materials science field, as they possess an unprecedented property combination of high strength and good ductility. 1,3-6 Wu et al.3 fabricated the HL structure in their Ti samples composed of nonuniform elongated micro and nano grain lamellae by asymmetric rolling and partial recrystallization. They claimed that the high strength and ductility observed in their HL samples were attributed to the high back-stress induced by the accumulation of dislocations in both soft and hard lamellae. Ma et al.^{4,5} produced the HL structure with NC bronze and coarse grain (CG) copper by high-pressure torsion, rolling, and annealing. They found that the HL sample can be deformed up

to 25% total strain without necking while the pure NC bronze sample can only sustain 3% tensile strain before fracture. Although the conventional rule of mixture (ROM) accurately predicted the yield strength, the HL sample exhibited an extra strain hardening that leads to larger uniform elongation than what is predicted by ROM. After analyzing the deformed sample, they claimed that the high ductility of the HL sample was related to extra geometrically necessary dislocations (GNDs) accumulated at the CG copper layer close to the interface. Nevertheless, it is still unclear whether the GNDs can form within the NC layer in the HL sample and how the NC layer can maintain such a high uniform elongation in HL samples.

Atomistic simulations can reveal the underlying mechanisms for the plastic deformation in NC materials as well as some specific phenomena that only appear at the nano-scale, such as the inverse Hall–Petch relation of the strength. ^{7–11} So far, there is no study on the deformation and fracture behaviors of heterogeneous lamella structures based on atomistic simulations. In this work, we performed molecular dynamics simulations on the heterogeneous NC Al lamellae composed of nanocrystalline

(NC) and single-crystalline (SC) layers to study the effect of heterogeneous microstructures on the deformation and fracture behavior of HL samples. After quantitative analysis, we found that the SC layer in the HL samples can release the stress concentration at the crack tip by emitting dislocations from the interface into the SC layer that can slow down the crack propagation rate and enhance the crack growth resistance.

Methodology and Model Setup

The samples used in our simulation are shown in Fig. 1. All samples have the same dimensions of $80 \times 103 \times 2 \text{ nm}^3$, and the crystalline orientation in the z direction is parallel to [110]. The grains with hexagonal shape are constructed by the modified Voronoi method. ^{12,13} Each grain was rotated around [110] (z) axis with a random angle. To minimize the influence of the misorientation between neighboring grains on the crack propagation behavior, we set the identical combination of orientations for the six grains ahead of the preexisting crack in all initial samples. That can help us make a quantitative comparison of the mechanical response between different samples. As shown in Fig. 1a, we set the initial crystallographic orientation as x-[111], y- $[\bar{1}1\bar{2}]$, and z-[110] and then rotated the grain number 1 to 6 by -45°, 90°, 0°, 0°, -45°, and 90° along [110] axis, respectively. This strategy was recommended by Wang et al. ¹⁴ in their recent atomistic simulations to reduce the random error induced by the randomly orientated grains. Figure 1a shows a pure NC sample containing 10-nm grains. The HL samples created by replacing 40%, 30%, and 20% volume of nano grains with a single crystal layer were named HL1, HL3, and HL2, respectively. Figure 1b and c present the structure of HL1 and HL2 samples. Therefore, the effect of the volume fraction of the SC layer on the mechanical response of the HL structure can be evaluated in our study. In addition, we also constructed the NC, HL1 and HL2 samples with 5-nm grains to explore the grain size effect on the crack propagation behavior, as shown in Fig. 1d, e and f. The crystallographic orientations of the SC layer were x- $[\bar{1}11]$, v-[$\bar{1}1\bar{2}$], and z-[110] for both HL1 and HL2 samples. To investigate the influence of orientation of the single crystal layer, we also created a second HL1 sample by rotating the SC layer 90° along the z-axis to make the x-axis parallel to [112] direction. All samples have the same initial crack configuration with the preexisting crack length equal to 33 nm, and the interaction between the atoms in two slabs were turned off based on the method provided in Ref. 15. Although no previous experimental studies reported the same microstructure presented in this work, the interface between the SC layer and the NC layer in the present work can mimic the transition region between the coarse-grain and nano-grain layers in the experimental samples,

such as for bimodal nanostructured materials, ¹⁶ heterogeneous lamella materials, ¹⁷ and gradient nanograined materials. ¹⁸ Therefore, the results from this study can be used to explore the corresponding fracture mechanisms.

The simulations were performed by using largescale atomic/molecular massively parallel simulator (LAMMPS) code¹⁵ with the embedded-atom method (EAM) potential for the Al system developed by Mendelev et al. 19 Periodic boundary conditions were imposed along the x and z directions, while the ydirection was set as a free boundary. Before loading, we used the conjugate gradient method to relax the sample first. After that, the samples were equilibrated at 300 K for about 50 ps by the Nose/Hoover isobaric-isothermal ensemble (NPT)^{20,21} and then slowly cooled to 10 K with the cooling rate about 0.1 K/ps. After relaxation, uniaxial tensile loading was applied on the x direction with a constant engineering strain rate of $5 \times 10^8 \text{ s}^{-1}$, and a time step was set as 1 fs. During the loading, the temperature was kept to 10 K and the pressure for the z direction was kept zero as the NPT system. Common neighbor analysis method (CNA),²² atomistic virial stress, and crack propagation distance were calculated to characterize the microstructure evolution during loading. The software OVITO was used to visualize the atomistic structure.²³

RESULTS AND DISCUSSION

Figure 2 shows the relationship between the strain and crack propagation distance for NC and HL samples with different grain sizes, volume fractions, and orientations of the SC layer. Figure 2a compares the results from samples containing 10-nm grains. It is obvious that the final propagation distance of a preexisting crack in all HL samples was smaller than that in the pure NC sample. The crack in the NC sample moved more than 50 nm for only 6% tensile strain, while the crack in all HL samples stopped at a distance less than 30 nm. These results indicate that the HL samples have better crack growth resistance than the NC sample. Moreover, the crack propagation distances in HL1 samples are even shorter than that in the HL2 sample. In the NC sample, the crack propagated continuously without stopping until reaching the final stage, while cracks in all HL samples grew intermittently and stopped much earlier than that in the NC sample. Although the preexisting crack started propagating in the HL2 sample at the same critical strain (3.5%) as that in the NC sample, the final distance was just about 20 nm shorter than that in the NC sample. In addition, the two HL1 samples delayed the critical strain to activate the preexisting crack from 3.5% to 4% and to shorten the crack propagation distance from 50 nm to 20 nm or less. After moving 15 to 20 nm, the crack in the HL1 samples fully stopped even with the incensement of external applied

62 Huang, Wang, and Zhou

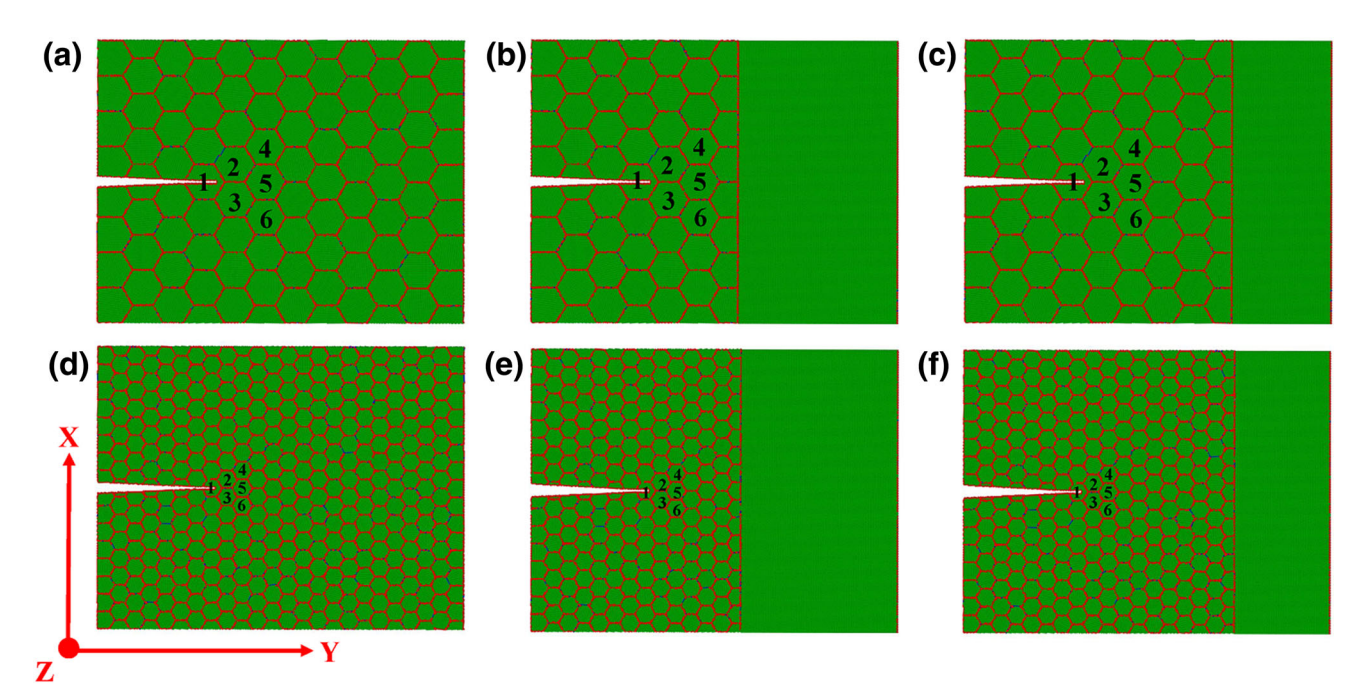


Fig. 1. Initial configuration of NC and HL samples: (a) 10-nm NC sample, (b) 10-nm HL1 sample with 40% volume fraction of single crystal, (c) 10-nm HL2 sample with about 20% volume fraction of single crystal. (d) 5-nm NC sample, (e) 5-nm HL1 sample with 40% volume fraction of single crystal, and (f) 5-nm HL2 sample with 20% volume fraction of single crystal. The crystallographic orientation of grains 1–6 in all samples were rotated along the z-[110] by -45° , 90°, 0°, 0°, -45° , and 90°, respectively. Other grains were rotated with random angles. (FCC and GB atoms are colored by green and read, respectively).

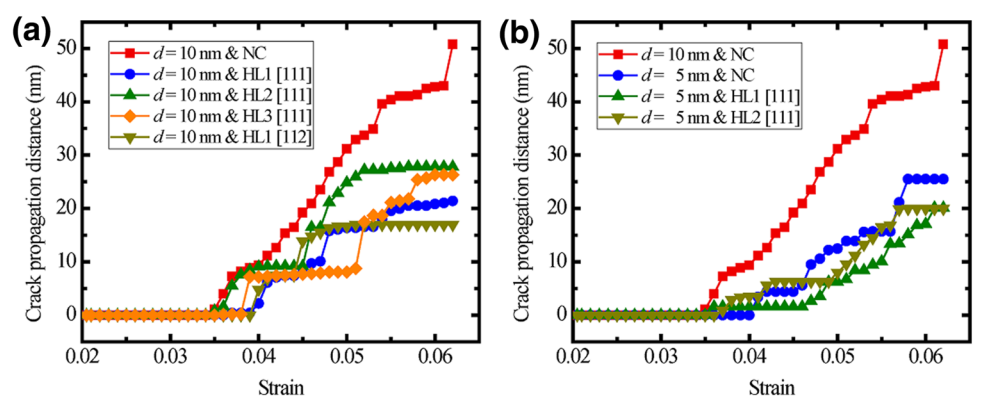


Fig. 2. Curves for crack propagation distance versus total strain on all samples with (a) 10-nm grains and (b) 5-nm grains.

strain. In addition, the crack propagation curves for HL1 [111] and HL1 [112] samples are very similar. It demonstrates that the influence from the crystallographic orientation of the SC layer on the crack propagation behavior in the HL sample is not as significant as the volume fraction of the SC layers.

Figure 2b plots the crack propagation curves for samples containing 5-nm grains. When compared with the pure 10-nm NC sample, all 5-nm samples exhibited better crack growth resistance with lower propagation rates and shorter distances. This can be attributed to the higher GB densities in 5-nm samples. Since the crack generally propagated along the GB, the higher density of GB forced the crack to

change propagation direction frequently and the crack propagation rate was reduced in the 5-nm samples. Several previous studies 24-26 also revealed similar phenomenon in NC materials that the fracture resistance or ductility increases when decreasing the grain size below 10 nm. In addition, Fig. 2b also illustrates that the heterogeneous structure in HL1 and HL2 samples containing 5-nm grains provided limited improvement in the resistance for the crack propagation as all three crack propagation curves cross each other. It is worth mentioning that this study just focused on the crack propagation behavior close to the interface in heterogeneous structures. In the future, more

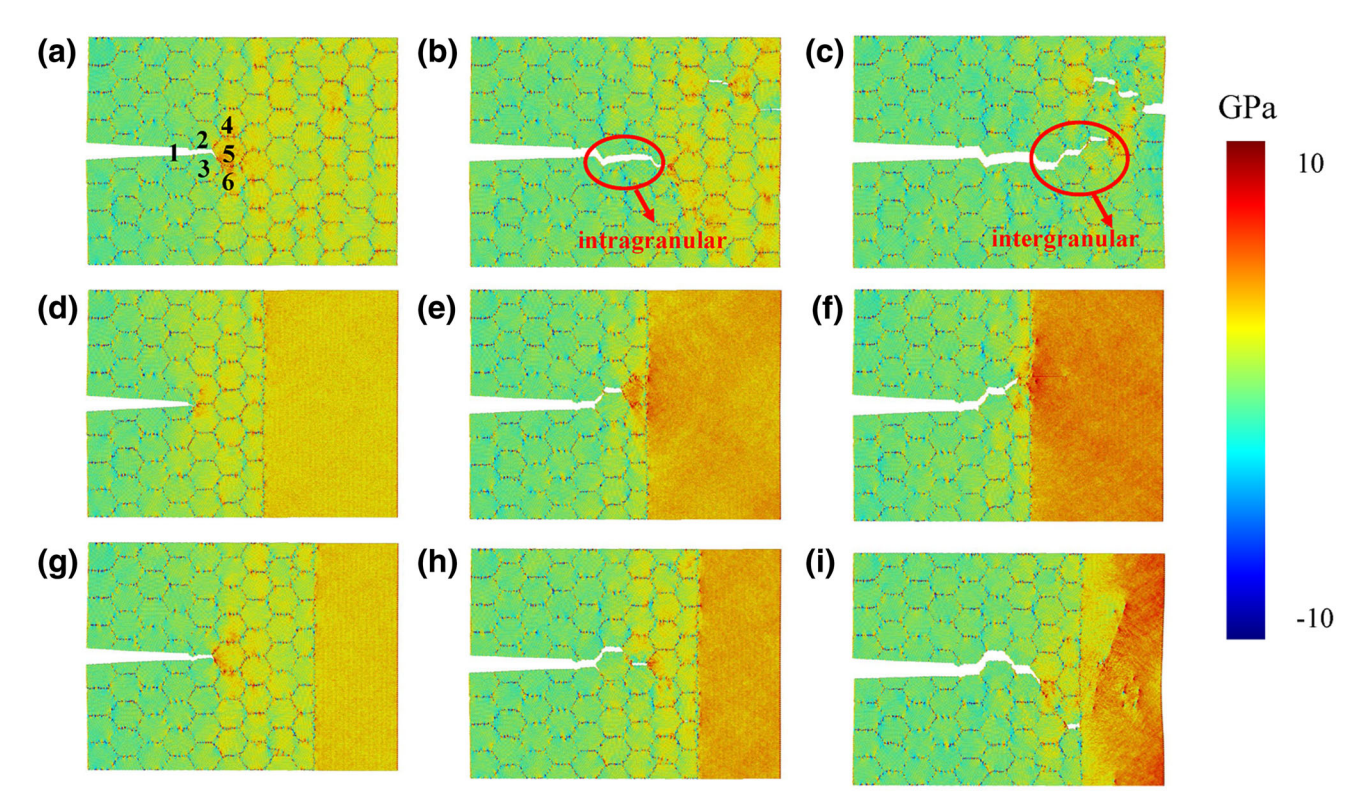


Fig. 3. Contour plots of atomistic virial stress, σ_{xx} , in samples with 10-nm grains: (a)–(c) NC sample at 4, 5, and 6% strain, respectively. (d)–(f) HL1 sample at 4, 5, and 6% strain, respectively. (g)–(i) HL2 sample at 4, 5, and 6% strain, respectively.

studies on large samples and various grain sizes are needed to study the effect of heterogeneous structures on the crack initiation and growth rate under different loading conditions.

Figure 3 presents the contour plots of the atomistic level virial stress σ_{xx} made at three different strain levels to explore the microstructure evolution in precracked samples. As a result of their higher stress, GB atoms are clearly visible. In addition, the local stress concentration at the crack tip is also visible under external loading. In the NC sample, the crack continuously propagated with the increase of the applied strain. As shown in Fig. 3a, the preexisting crack propagated along the GB between grain 2 and grain 3 and then changed the propagation direction along the GB between grain 3 and grain 5. Nevertheless, if the GBs have a higher fracture resistance and the local stress is high enough to make the crack propagate within the grain interiors, the fracture mode may transform from intergranular into intragranular mode. In Fig. 3b, the crack did not propagate along the GB between grain 5 and grain 6 but propagated within grain 5, which is the intragranular mode. After the intragranular propagation within two grains, the crack propagated along the GBs again, which is the intergranular mode as shown in Fig. 3c. At the same time, new cracks at the right side of the sample formed at 5% applied strain in Fig. 3b. The nucleation of new cracks in the NC sample was

caused by the highly heterogeneous deformation in neighboring grains. In NC materials, there is little chance to form GNDs within the nano grains to accommodate the plastic incompatibility across the boundary, as the mobile dislocation normally nucleates from one GB and glides across the grain without any interaction with other dislocations and the mean free path for mobile dislocations is limited by the grain size. ^{27–30} The new cracks formed in the NC sample continuously propagate along the GBs to relax the elastic energy stored at the crack tip that prohibited the preexisting crack growth as shown in Fig. 3c. This event corresponds to the flat region between 5% and 6% strain on the crack propagation curve for the NC sample in Fig. 2a. Figure 3d, e, f, g, h and i illustrate the microstructure evolution of HL1 and HL2 samples, respectively. From the contour plots, we can see that the stress distribution in SC layers is uniform compared with that in the NC layer as the stresses on GBs are normally much higher than that within the grains in the NC layer. More importantly, there is no or few newly formed cracks in the HL samples, especially in the HL1 sample. This is consistent with the results from our previous studies, in which we demonstrated that the SC layer can homogenize the plastic deformation within the NC layer in HL samples and suppress the crack nucleation probability.²⁷ In addition, the HL1 sample with a lower volume fraction of NC layers possessed better crack

Huang, Wang, and Zhou

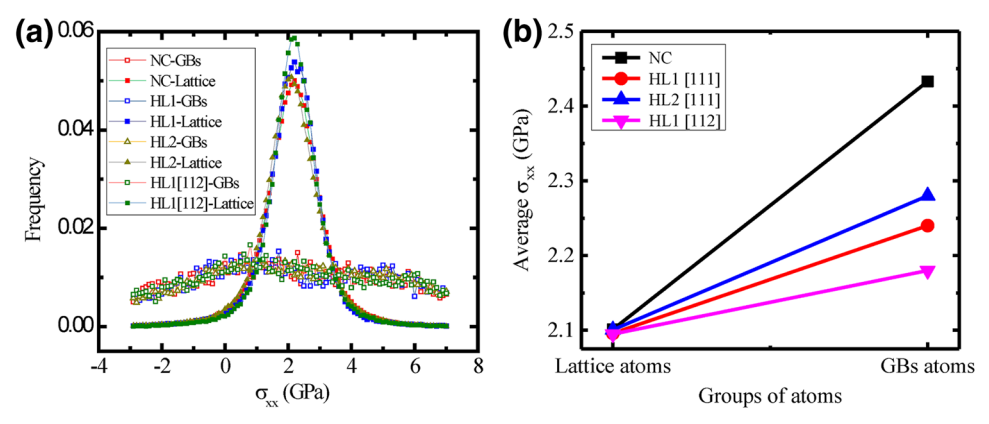


Fig. 4. (a) Distribution of the σ_{xx} among GB and lattice atoms in different samples. (b) Comparison between the average σ_{xx} of GB and non-GB atoms.

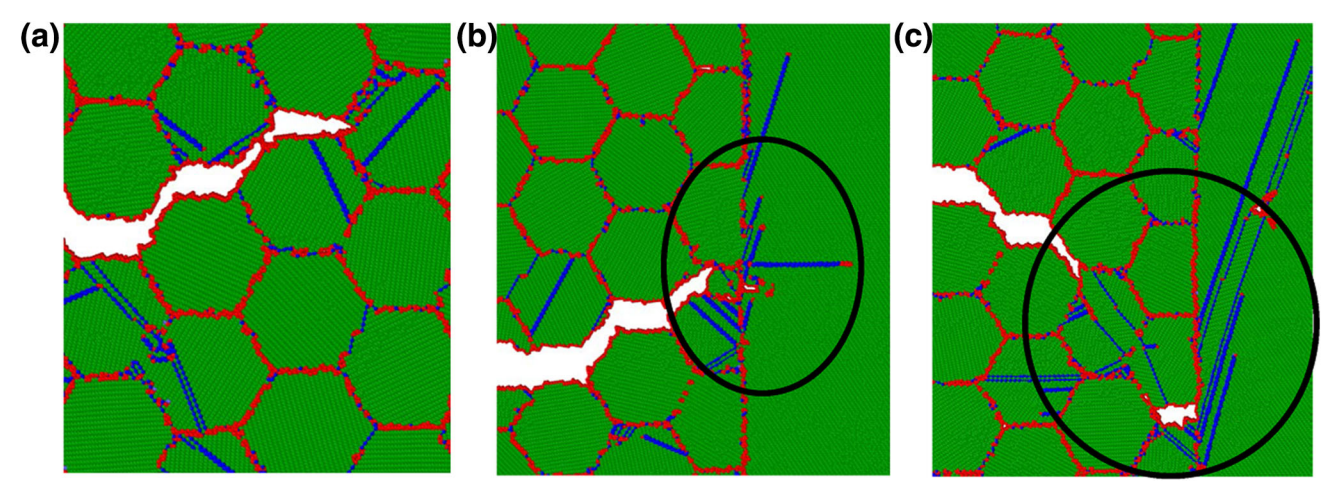


Fig. 5. Atomistic structures at 6% total strain around the crack tip for samples containing 10-nm grains: (a) NC (b) HL1, and (c) HL2. Atoms colored by the CNA methods. (Atoms with green, blue, and red represent the FCC, HCP, and unknown atoms, respectively. The unknown atoms in these figures generally represent the atoms located on grain boundaries).

resistance, which also agrees with the experiment results on HL structures that shows the uniform elongation increases with the decrease of volume fraction of the NC layer.^{4,5}

To analyze the atomistic level virial stress quantitatively, the stress in the tensile loading direction, σ_{xx} , of the GB and lattice atoms at the front of the preexisting crack were calculated separately. The width of the analyzed region is about one-fifth of the width of the sample from the crack tip. Thus, the analyzed GB atoms are far away from the right boundary and the influence from the free surface has been minimized. From Fig. 4a, we can see the average stresses on lattice atoms follow the normal distribution in all three cases with sharp peaks at the stress around 2.0 GPa. Meanwhile, the stress distributions for GB atoms are flat and spread out without obvious peaks. Thus, the local stresses on GB atoms are more heterogonous than those on lattice atoms. Nevertheless, it is hard to differentiate the stress distributions from one case to another case. Thus, Fig. 4b compares the average stresses

on the GB and on lattice atoms for three different cases. We can see that the average stresses on GB atoms were higher than the averages of lattice atoms in all three cases. Yet the HL structures can bring down the stress on GB and make it close to the stress on lattice atoms as shown in Fig. 4b. This can be used to explain the lower crack propagation rate in the HL samples observed in our simulations, as a larger external stress is needed to open the crack at GBs in the HL sample.

To better understand the microstructure evolution during deformation, the atomistic structures near the crack tip in NC, HL1, and HL2 samples with 10-nm grains were plotted in Fig. 5a, b and c. As shown in Fig. 5b and c, the dislocation activities were abundant near the interface between the NC layer and the SC layer in the HL samples, while the dislocation activities were limited in the NC sample at the crack tip region (Fig. 5a). As the motion of dislocations can release the elastic energy stored at the crack tip and reduce the local stress on GB atoms, the dislocation activities in HL samples

largely suppressed the propagation of preexisting cracks and improved the crack growth resistance. Recently, Wang et al. 14 performed atomistic simulations of gradient nano-grained Ni and attributed the enhanced ductility in the gradient nano-grained Ni to the transformation of fracture modes from intergranular to intragranular when the crack enters the larger grains. Here, the enhanced fracture resistance in our HL samples was not mainly induced by the transformation of fracture modes but by the emitting and gliding of the dislocations from the interface into the SC layer, which provided a large mean free path for the motion of dislocations that released the elastic strain energy at the crack tip alternatively. 31

CONCLUSION

In summary, molecular dynamics simulations were performed on heterogeneous NC Al lamellae to explore the effect of the heterogeneous microstructure on the propagation of preexisting cracks. Under tensile loading, the heterogeneous NC Al lamella exhibit higher crack growth resistance than the pure NC Al. After quantitative analysis, we found that the crack propagation rate was reduced in HL samples and that the average stress on GB atoms was much lower than that in pure NC sample. When the crack approaches the interface, the heterogeneous microstructure can reduce the stress concentration by emitting dislocations from the interface into the SC layer. In addition, the crack growth resistance in HL samples increases with the decrease of the volume fraction of NC layers, which is consistent with previous experiment results. Furthermore, the relative uniform deformation in the SC layer can homogenize the plastic deformation in the NC layer and suppress the strain localization and crack nucleation. Our findings in this study can provide basic information for understanding the mechanics of heterogeneous structures and for evaluating their performance.

ACKNOWLEDGEMENTS

This work was supported by Grants from NSF CAREER Award (CMMI-1652662). S.H. is also grateful for the partial support provided by The University of Missouri Research Board. J.W. also appreciates the financial support received from the National Natural Science Foundation of China

(NSFC: 51308474). The supercomputer time allocation for completing the atomistic simulations was provided by the Extreme Science and Engineering Discovery Environment (XSEDE), Award No. DMR170093.

REFERENCES

- 1. T.G. Langdon, Acta Mater. 61, 7035 (2013).
- R. Valiev and I. Alexandrov, Nanostruct. Mater. 12, 35 (1999).
- X. Wu, M. Yang, F. Yuan, G. Wu, Y. Wei, X. Huang, and Y. Zhu, Proc. Natl. Acad. Sci. USA 112, 14501 (2015).
- X. Ma, C. Huang, W. Xu, H. Zhou, X. Wu, and Y. Zhu, Scripta Mater. 103, 57 (2015).
- X. Ma, C. Huang, J. Moering, M. Ruppert, H.W. Höppel, M. Göken, J. Narayan, and Y. Zhu, Acta Mater. 116, 43 (2016).
- 6. E. Ma and T. Zhu, Mater. Today 20, 323 (2017).
- 7. J. Schiøtz and K.W. Jacobsen, Science 301, 1357 (2003).
- 8. V. Yamakov, D. Wolf, S. Phillpot, A. Mukherjee, and H. Gleiter, *Nat. Mater.* 3, 43 (2004).
- 9. C. Deng and F. Sansoz, Appl. Phys. Lett. 95, 091914 (2009).
- S. Huang, I. Beyerlein, and C. Zhou, Sci. Rep. 7, 11251 (2017).
- 11. S. Huang and C. Zhou, JOM 69, 2256 (2017).
- V. Yamakov, D. Wolf, M. Salazar, S. Phillpot, and H. Gleiter, Acta Mater. 49, 2713 (2001).
- 13. D. Chen, Mater. Sci. Eng. A 190, 193 (1995).
- P. Wang, X. Yang, and X. Tian, J. Mater. Res. 30, 709 (2015).
- S. Plimpton, J. Comput. Phys. 117, 1 (1995).
- Y. Zhao, T. Topping, J.F. Bingert, J.J. Thornton, A.M. Dangelewicz, Y. Li, W. Liu, Y. Zhu, Y. Zhou, and E.J. Lavernia, Adv. Mater. 20, 3028 (2008).
- X. Wu, P. Jiang, L. Chen, F. Yuan, and Y.T. Zhu, Proc. Natl. Acad. Sci. USA 111, 7197 (2014).
- 18. T. Fang, W. Li, N. Tao, and K. Lu, Science 331, 1587 (2011).
- M. Mendelev, M. Kramer, C.A. Becker, and M. Asta, *Philos. Mag.* 88, 1723 (2008).
- 20. W.G. Hoover, Phys. Rev. A 34, 2499 (1986).
- 21. S. Nosé, J. Chem. Phys. 81, 511 (1984).
- J.D. Honeycutt and H.C. Andersen, J. Phys. Chem. 91, 4950 (1987).
- A. Stukowski, Model. Simul. Mater. Sci. Eng. 18, 015012 (2009)
- 24. D. Farkas, Metall. Trans. A 38, 2168 (2007).
- M.A. Meyers, A. Mishra, and D.J. Benson, *Prog. Mater Sci.* 51, 427 (2006).
- 26. T. Zhu and J. Li, Prog. Mater Sci. 55, 710 (2010).
- R. Yuan, I.J. Beyerlein, and C. Zhou, *Mater. Res. Lett.* 5, 251 (2017).
- M. Ardeljan, M. Knezevic, T. Nizolek, I.J. Beyerlein, N.A. Mara, and T.M. Pollock, J. Appl. Phys. 74, 35 (2015).
- R. Yuan, I.J. Beyerlein, and C. Zhou, Acta Mater. 90, 169 (2015).
- R. Yuan, I.J. Beyerlein, and C. Zhou, *Acta Mater.* 110, 8 (2016)
- 31. E. Bitzek and P. Gumbsch, *Acta Mater.* 61, 1394 (2013).